Rolling contact fatigue behavior of dual-phase austempered ductile iron

Diego A. Colombo, Ricardo C. Dommarco, Alejandro D. Basso

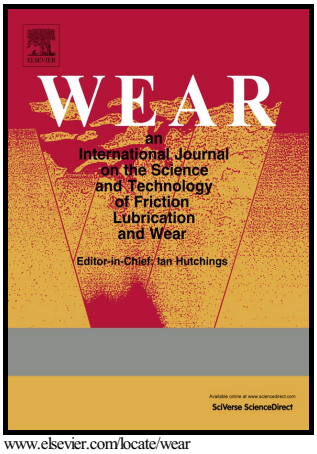

www.elsevier.com/locate/wear

PII: S0043-1648(18)30897-4
DOI: https://doi.org/10.1016/j.wear.2018.11.009
Reference: WEA102544

To appear in: *Wear*

Received date: 24 July 2018
Revised date: 19 October 2018
Accepted date: 18 November 2018

Cite this article as: Diego A. Colombo, Ricardo C. Dommarco and Alejandro D. Basso, Rolling contact fatigue behavior of dual-phase austempered ductile iron, *Wear,* https://doi.org/10.1016/j.wear.2018.11.009

Rolling contact fatigue behavior of dual-phase austempered ductile iron

Diego A. Colombo*, Ricardo C. Dommarco, Alejandro D. Basso

Instituto de Investigaciones en Ciencia y Tecnología de Materiales, UNMdP, CONICET,

Facultad de Ingeniería, Av. J. B. Justo 4302, B7608FDQ Mar del Plata, Argentina

* Corresponding author:

Phone: +54-223-481-6600 ext. 260

Fax: +54-223-481-0046

E-mail address: diegocolombo@fi.mdp.edu.ar

Abstract

In this work the rolling contact fatigue (RCF) behavior of dual-phase austempered ductile iron (ADI) was studied and compared to that of conventional ADI. The effect of surface finishing (manual vs. automatic grinding) on the surface properties and RCF endurance was also analyzed. RCF tests were performed in a flat washer type testing rig and using lubricated pure rolling conditions. RCF tests results were analyzed using the two-parameter Weibull distribution and the Weibayes method.

The results indicated that the dual-phase ADI metal matrix was composed of 94 % ausferrite and 6 % free allotriomorphic ferrite, approximately. The hardness of conventional ADI was higher than that of dual-phase ADI. The residual stresses were compressive in all the cases with similar average values for ADI and dual-phase ADI. Relative to manual grinding, the automatic process increased slightly the surface hardness and reduced by around a 50 % the

residual stresses of both ADI and dual-phase ADI. Regarding RCF, failures were characterized by the typical concentrated damage in the form of spalls. No significant differences in the RCF endurance of ADI and dual-phase ADI were observed. No differences in the RCF endurance attributable to the surface finishing method were identified in the current tests.

Keywords: dual-phase austempered ductile iron, grinding, surface properties, rolling contact fatigue.

1. Introduction

Ductile iron (DI) is an attractive engineering material for the manufacturing of mechanical components due to the advantages of the near net shape technology and the wide range of mechanical properties that is possible to obtain through a suitable microstructural adjustment, both in the as-cast condition or by means of heat treatments [1]. The most widely used heat treatments for DI is austempering, which produces the so called austempered ductile iron (ADI). ADI has attracted considerable interest in the last decades because of its excellent combination of high strength and ductility with good wear resistance [2-5]. In addition, the manufacturing cost, recyclability, density, fluidity, damping capacity, heat conductivity and lubricity of either DI or ADI are better than that of forged or cast steels, and therefore they are considered as an economical substitute for these materials in many applications.

ADI is commonly used for the manufacturing of mechanical components subjected to rolling or rolling/sliding contacts, such as gears and cams. A major cause of failure in this type of components is rolling contact fatigue (RCF). RCF can be defined as the mechanism of crack nucleation and propagation caused by the near surface alternating stress field within the

contact bodies, which eventually leads to material removal by a spall or crater formation. Several authors have studied the RCF behavior of ADI [6-10], finding that its sensitivity to damage increases as austempering temperature and holding time decrease and as nodule count increases, and that surface and subsurface graphite nodules act as preferential sites for crack nucleation. The influence of specimen preparation on the RCF behavior of ADI has also been studied [11], finding that a polishing with 1 μm diamond grains after grinding process led to a decrease of surface roughness and an increase in RCF life. Other authors have studied the effects of different surface treatments [12, 13], finding that a laser hardening, which induced a near surface structure transformation, increased the RCF life of ADI and that a shot peening, which induced compressive residual stresses but also increased surface roughness, was not beneficial. Laser hardening produced a near surface structure of about 1 mm thick composed of martensite needles and retained austenite which was ascribed to the better RCF behavior.

In the last years a new type of DI, called dual-phase ADI or IDI (intercritical ductile iron) was developed. The matrix of dual-phase ADI is composed of ausferrite (regular ADI microstructure) and free (or allotriomorphic) ferrite, which is obtained by subjecting DI to special heat treatments. Several studies have focused on determining the mechanical response of dual-phase ADI [14-20]. The results have revealed that it can offer a wide range of mechanical properties depending on the relative percentage of microconstituents present in the matrix. For instance, dual-phase ADI with a predominantly ausferritic microstructure (90-95 % ausferrite) displayed tensile strength and yield stress values similar to those of ADI, but showed higher values of deformation at failure and mode I fracture toughness (K_{IC}) [15]. This kind of dual-phase ADI microstructure could offer a potential replacement to ADI in several applications. More recently, the sliding wear behavior of dual-phase ADI was studied [21], finding that a predominantly ausferritic microstructure reduces friction coefficient and wear

rate. However, to the best of the authors' knowledge, there is no information available regarding the RCF performance of dual-phase ADI.

Several authors have studied the mechanisms of RCF crack propagation under lubricated contacts. Three basic models driving crack propagation have been proposed [22-27], one is mainly attributed to shear stresses, other is the hydraulic pressure mechanism and the last one is the fluid entrapment theory. These models indicate that mixed mode stress intensity factors of mode I (opening) and mode II/III (shear) act at a crack tip [28, 29]. A more recent study developed a coupled fluid/solid elastohydrodynamic model [30], finding that RCF crack propagation is driven by mode I stress intensity. Since dual-phase ADI exhibits a higher mode I fracture toughness than conventional ADI [15], a RCF endurance at least similar to that of conventional ADI would be considered a promising result given that dual-phase ADI shows improvements in other properties such as ductility, friction coefficient and wear rate.

On the other hand, there are some applications in which good surface finish and accurate dimensional tolerances are mandatory. As a consequence, high precision machining processes are required, grinding being one of the most suitable and used processes. The abrasive cutting process involved in grinding produces a plastically deformed surface layer (mechanical effect). Depending on the material and grinding conditions (wheel characteristics, workspeed, wheelspeed, depth of cut, use of coolant) it could also produce high temperatures in the workpiece-wheel contact area (thermal effect) [31]. As a result, the surface properties of the material (hardness, roughness, residual stresses and microstructure) could be altered which, in turn, may affect its bearing capacity, wear behavior and fatigue resistance. Regarding residual stresses, the mechanical effect leads to compressive stresses while the thermal effect to tensile stresses. Consequently, the combined effect of material and grinding conditions will lead to compressive, tensile or null residual stresses [31].

The main outcomes of the bibliographic references cited suggest that the RCF behavior of ADI could vary with the presence of small amounts of dispersed ferrite in the ausferritic matrix and also with surface roughness, surface hardness and near-surface residual stresses. On this basis, the aim of the present work is to study the RCF behavior of dual-phase ADI with a predominantly ausferritic microstructure (90-95 % ausferrite) and to evaluate the effect of surface finishing (manual vs. automatic grinding) on its surface properties and RCF endurance. Conventional ADI samples are also tested for comparative purposes.

2. Experimental procedures

2.1. Casting material and samples preparation

The DI utilized in this work was produced in a 55 kg middle-frequency induction furnace (3 kHz). The melt was conventionally nodulized and inoculated [32] and then it was poured into horizontal sand moulds designed to obtain 70 mm diameter and 10 mm thick discs. The chemical composition of the DI, analyzed by optical emission spectrometry, was as follows: C= 3.22; Si= 2.58; Mn= 0.29; S= 0.02; P= 0.04; Mg= 0.04; Cu= 0.69; Ni= 0.40 and Fe balanced in wt. %. The average nodule count and nodule diameter of the DI were about 285 nod/mm^2 and 15 µm, respectively. Nodularity exceeded 95 % in all cases. These microstructural characteristics were evaluated according to the ASTM A247 standard [33]. The discs were cut from the castings and machined to obtain samples with a final size of 65 mm in diameter and about 8 mm in thickness.

2.2. Heat treatments

2.2.1. Annealing heat treatment

As mentioned in the literature [15-20], in the first stage, samples destined to produce dual-phase ADI structures were annealed in order to obtain a fully ferritic matrix (starting microstructure). Thermal cycle consisted in a fully austenitizing at 910 ºC for 6 hours in electric furnace, cooling down to 740 ºC inside the furnace, holding at 740 ºC for 10 hours and cooling down to room temperature inside the furnace.

2.2.2. Determination of the intercritical interval

To obtain a dual-phase ADI microstructure with specific amount of phases (ferrite and ausferrite) it is necessary to determine firstly the intercritical interval of the alloy, which depends strongly on its chemical composition. The intercritical interval was determined by employing the methodology described in previous works by the authors [15, 17, 18], which is summarized as follows: ferritized samples were subjected to thermal cycles involving austenitizing stages at temperatures ranging from 700 to 920 ºC, at steps of 20 ºC. Each complete thermal cycle consisted of holding the sample for 1 hour in the furnace at each selected temperature (Tγ). After the heating stage, samples were water quenched. The resulting microstructures were composed of different amounts of ferrite (original matrix) and martensite (quenched austenite). It is important to point out that, based on previous works, a holding time of about 30 min in the heating step is enough to reach the equilibrium phase percentages in the $\alpha \rightarrow \gamma$ transformation within the intercritical interval, starting from fully ferritic matrices.

The characterization of the intercritical interval allows determination of the upper and lower critical temperatures and the amount of phases (ferrite and austenite) as a function of austenitizing temperature.

2.2.3. Heat treatments to produce ADI and dual-phase ADI structures

The thermal cycle used to obtain dual-phase ADI microstructures consisted in a first step of intercritical or partial austenization by holding the samples in the furnace at temperatures within the intercritical interval previously determined, followed by an austempering step in a salt bath. To obtain a microstructure with a percentage of ausferrite of about 90-95 %, an intercritical austenitizing at 850 ºC for 3 hours was performed. This stage was followed by an austempering step at 280 ºC for 2 hours. The thermal cycle used to obtain fully ausferritic (conventional ADI) samples consisted in a complete austenitizing step at 910 ºC for 3 hours, followed by an austempering at the same temperature and time as the dual-phase ADI samples. Figure 1 shows a schematic of the thermal cycles used to obtain ADI and dual-phase ADI microstructures.

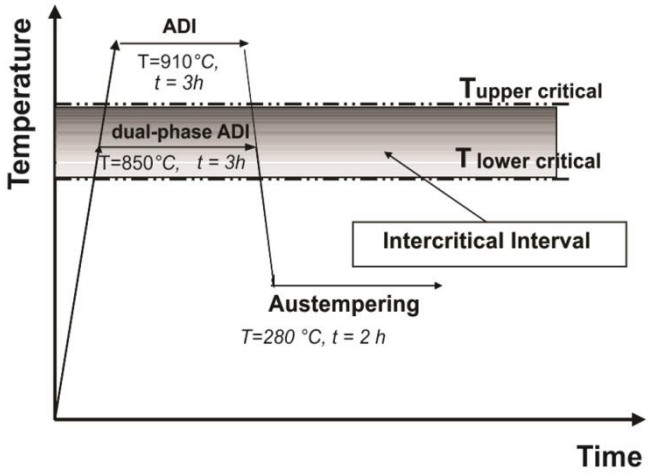

Figure 1. Schematic of the thermal cycles used to obtain ADI and dual-phase ADI microstructures

2.3. Surface finishing

The treated samples were subjected to two different surface finishes, manual and automatic grinding, i.e., low and high energy processes, respectively. Automatic grinding was carried out using a peripheral surface grinder equipped with horizontal spindle and reciprocating table. Three roughing passes and one finishing pass were conducted on each sample, with depths of cut of 0.03 and 0.01 mm, respectively. The finishing pass aims to attain a low surface roughness. Workspeed and wheelspeed values were kept in 26 m/min and 30 m/s, respectively. A grinding wheel made of SiC abrasive grains and vitrified binder was utilized. An oil-in-water emulsion was used as coolant. Manual grinding was performed using SiC waterproof paper. Compared to automated grinding operations, manual grinding is a poorly controlled process that is critically dependent on worker's skills and personal strength. For that reason, surface roughness was used as an index of process control stability. In addition, surface roughness plays an important role on RCF behavior [34]. Successive passes with papers of descending grit size were performed until reaching arithmetic average roughness (Ra) values similar to those of the automatic ground samples. Final grit size was 220 for ADI and dual-phase ADI samples. Manual ground samples were identified as "ADI – MG" and "dual-phase ADI – MG" while automatic ground samples as "ADI – AG" and "dual-phase ADI – AG".

2.4. Samples characterization

Metallographic samples were prepared by using standard techniques. Metallographic etching was performed with 2 % Nital. The microstructures were analyzed using an optical microscope, and the proportions of the phases in each sample were quantified by means of image software. Brinell hardness was evaluated using a 2.5 mm diameter tungsten carbide ball as an indenter with a 187.5 kg applied load ($HBW_{2.5/187.5}$). A microindentation tester equipped with a Knoop indenter was used to measure the surface hardness (15 g load, $HK_{0.015}$). The surface topography was analyzed using a stylus profilometer with a 4 mm evaluation length (cut-off, 0.8 mm). Near-surface residual stress measurements were conducted by x-ray diffraction (XRD) using the $\sin^2\psi$ method. A θ-θ diffractometer was utilized, with Cu Kα radiation (λ = 1.5418 Å) at 40 kV and 40 mA. Measurements were performed in the parallel direction to the grinding scratches at a radial distance of aproximately 15 mm from the centre of the samples. The gauge volume was estimated in 0.5 mm^3, with an average penetration depth of 8 μm. The optimal diffraction peaks for measurements were Fe-α (222). The 2θ angle ranged from 134° to 140°. Stresses were calculated using the x-ray elastic constants (XEC's) of Fe-α [35].

2.5. Rolling contact fatigue tests

RCF tests were performed in a flat washer type testing rig. A detailed description of the test machine was presented elsewhere [36]. A standard 51107 thrust ball bearing was used as a counterpart. The rotational speed of the samples was set at 1650 rpm, establishing a loading frequency of $1x10^6$ cycles/hour. Hydraulic oil with a kinematic viscosity of 100 cSt at 40 °C was used as lubricant. The maximum contact pressure (p_0) must be high enough so as to cause material degradation by microplasticity, but not that high so as to cause material build up along the edges of the rolling track [37, 38]. According to a previous study [39], the

maximum contact pressure (p_0) was set at 1400 MPa. The corresponding normal load and depth of maximum shear stress were calculated according to the Hertz contact theory as a reference, which resulted in 260 N and 30 μm respectively. The minimum oil film thickness (h_0) was 0.3 μm, as calculated by using the Hamrock and Dowson equation [40]. The specific oil film thickness parameter (λ) of ADI and dual-phase ADI samples was close to 1.2, resulting in a mixed lubrication regime where the surfaces are separated by a thin lubricant film but asperity contact also takes place. This regime predicts an increased probability of crack nucleation at the surface of the samples.

Eight RCF tests were carried out for each sample set. The samples were loaded until a macroscopic fatigue failure was produced on their surface or until reaching 200 hours of testing without failure (suspension). The time to failure of the samples was measured by an hour meter and converted into loading cycles. The rolling track of the samples was examined by scanning electron microscopy (SEM).

RCF results were analyzed using the two-parameter Weibull distribution. Suspensions are not displayed in the Weibull plots but they are included in the analyses. Life data were fitted by rank regression [41]. Life data were subjected to a statistical analysis in order to make inferences. Two-sided 90 % confidence intervals for each sample set were determined by the Weibayes method [41, 42], assuming the Weibull shape parameter (β) in the Weibayes solution.

3. Results and discussion

3.1. Microstructural characterization

Figure 2 shows the microstructures obtained for conventional ADI and dual-phase ADI samples. Conventional ADI (Figures 2a and 2b) possesses a fully ausferritic microstructure composed of a fine mixture of acicular ferrite and metastable austenite of high carbon content, in agreement with the low austempering temperature employed. On the other hand, the dual-phase ADI microstructure (Figures 2c and 2d) is composed of 94 % ausferrite and 6 % free allotriomorphic ferrite approximately (light regions), as expected. From Figure 2c it can be seen that ferrite is present as a dispersed microconstituent in the ausferritic matrix. The average Brinell hardness obtained for ADI and dual-phase ADI was about 410 and 390 $HBW_{2.5/187.5}$, respectively. Predictably, free allotriomorphic ferrite induces a slightly lower hardness in dual-phase ADI.

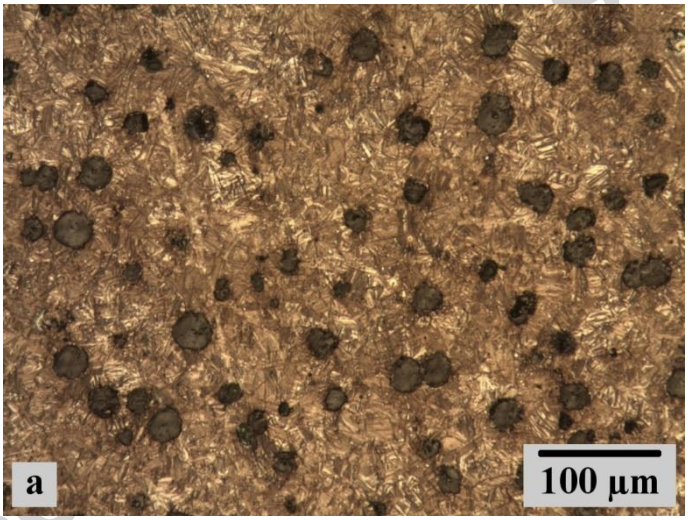

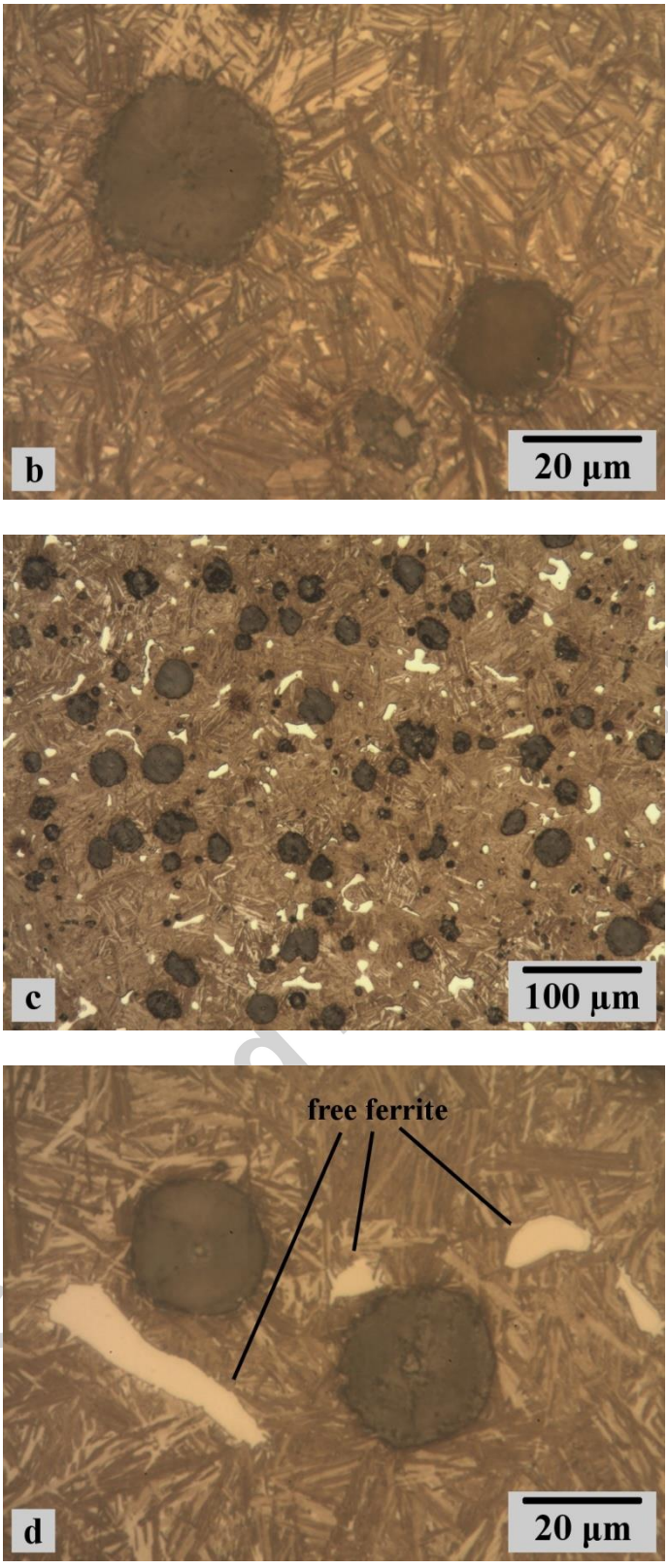

Figure 2. Microstructure of ADI and dual-phase ADI samples: (a) ADI magnification 100x, (b) ADI magnification 500x, (c) dual-phase ADI magnification 100x, (d) dual-phase ADI magnification 500x

3.2. Surface properties

Figure 3 shows, as an example, micrographs of the manual and automatic ground surfaces corresponding to ADI samples. Surface nodules can be seen in the manual ground surface and some of them may have present partial or complete graphite removal due to their practically null mechanical resistance [32]. On the other hand, surface nodules cannot be seen in the automatic ground surface due to the plastic deformation of the metallic matrix, inherent to the abrasive cutting of grinding, which covers the nodules.

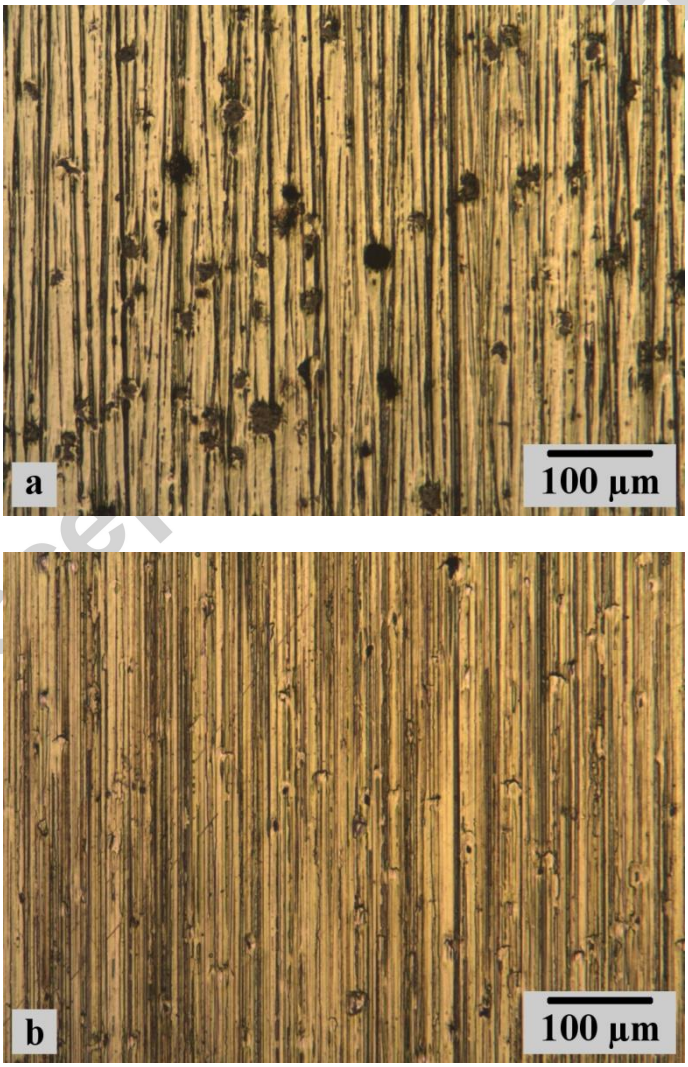

Figure 3. Micrographs of the surfaces corresponding to ADI samples: (a) manual ground, (b) automatic ground

Table 1 reports the surface properties of ADI and dual-phase ADI samples.

Table 1. Surface properties of ADI and dual-phase ADI

Sample	Arithmetic average Roughness, Ra (μm)	Hardness ($HK_{0.015}$)	Residual stress (MPa)
ADI – MG	0.254 ± 0.062	837 ± 62	-799.9 ± 50.1
ADI – AG	0.246 ± 0.031	904 ± 72	-401.6 ± 29.5
Dual-phase ADI – MG	0.241 ± 0.037	706 ± 107	-812.6 ± 39.4
Dual-phase ADI – AG	0.267 ± 0.027	780 ± 62	-378.7 ± 77.2

According to what was intended, the mean and dispersion of Ra parameter are similar for ADI and dual-phase ADI and for both surface finishing methods. The average surface hardness of conventional ADI is higher than that of dual-phase ADI, due to the presence of free ferrite in the latter. In addition, the surface hardness increased slightly with the automatic grinding process. This behavior can be ascribed to the relatively high bulk hardness of both materials, which limit the deformation capacity and restrict the plastically deformed layer to approximately one half of the depth of cut (≈ 5 μm) [31]. This can be observed in Figure 4, on a cross section parallel to the automatic grinding direction on an ADI sample. In addition, the presence of martensite in areas with traces of plastic deformation could not be determined metallographically.

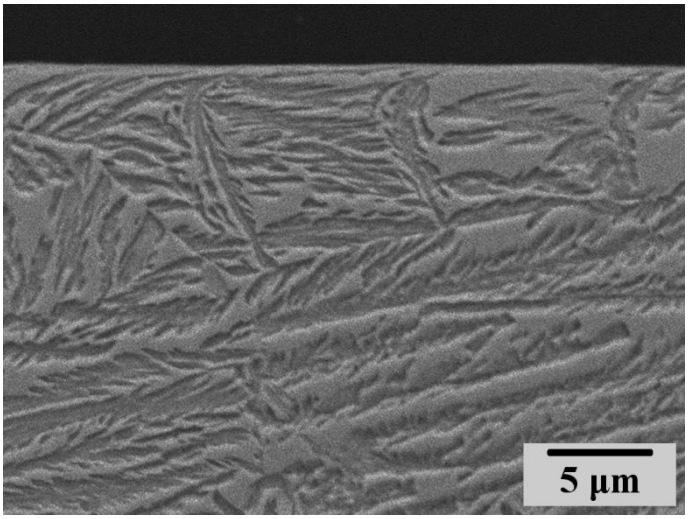

Figure 4. Cross section micrograph of an automatic ground ADI sample

The residual stresses are compressive in all the cases and are not influenced by the microstructure (similar average values for ADI and dual-phase ADI). However, residual stresses vary with the surface finishing method employed. The values of the manual ground samples are close to -800 MPa. According to a previous work [43], this level of residual stresses can be ascribed mainly to the austempering heat treatment. The values of the automatic ground samples are close to -400 MPa. The reduction in the residual stress level can be ascribed to the cutting conditions employed [31], which cause that the thermal effect predominates over the mechanical effect.

3.3. Rolling contact fatigue behavior

As stated before, the contact load applied to the test samples should be enough to cause material damage by microplasticity but not too high to cause material build up along the edges of the rolling track (RT). Figure 5 shows, as an example, the RT profile of one of the dual-phase ADI – MG samples, i.e. those with lower hardness, after $\approx 50 \times 10^6$ cycles. It can be seen that the profile does not reveal material build up along the edges of the RT and that the width is various

orders of magnitude higher than the depth of the RT, indicating that there is not a noticeable modification of the contact geometry and that the results are valid.

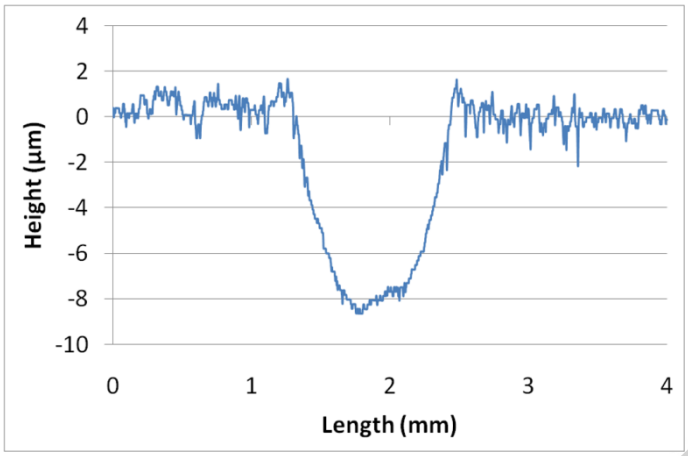

Figure 5. Rolling track profile of dual-phase ADI – MG

Figure 6 illustrates the RCF failures observed in ADI and dual-phase ADI. The rolling direction (RD) is indicated on the images. Failures were characterized by the typical concentrated damage in the form of spalls. It can be seen that spalls exhibit an irregular morphology on all sample variants, due to the fact that crack path is strongly influenced by the nodules present at and under the surface. According to the calculated λ parameter which predicted asperity interaction of the contact bodies, micrographs showing a sequence of a RCF spall development from a surface origin are presented in Figure 7. In addition, it also was observed that some spalls appeared suddenly within the RT which can be ascribed to subsurface crack nucleation and propagation [6, 11]. Figure 8 shows, as an example, some scratches inside the RT of ADI – AG oriented along the RD, indicating the aforementioned asperity interaction.

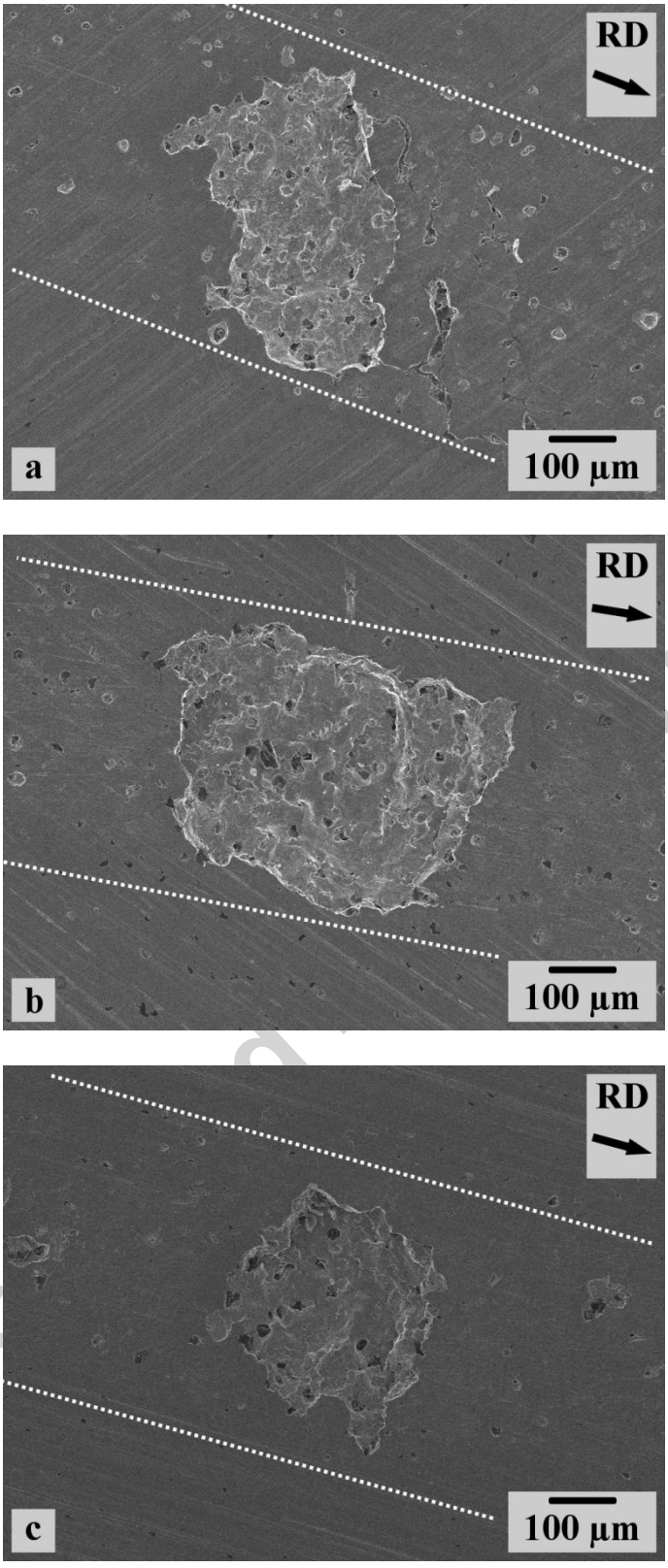
RD
a
100 µm
RD
b
100 µm
RD
c
100 µm

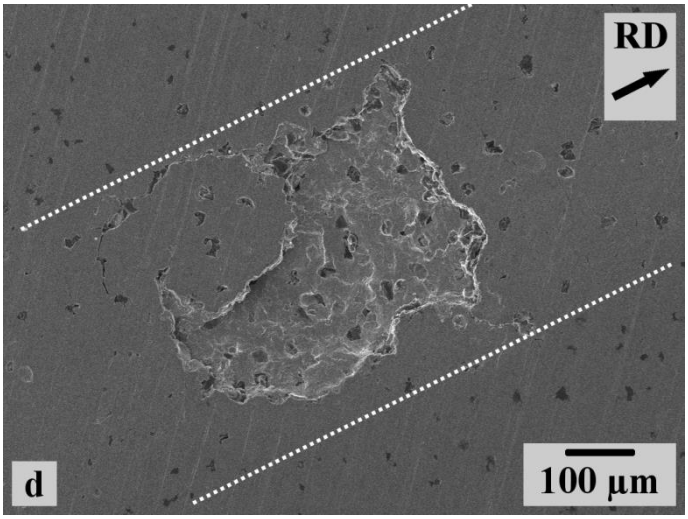

Figure 6. RCF failures observed in ADI and dual-phase ADI samples: (a) ADI – AG, (b) ADI – MG, (c) dual-phase ADI – AG, (d) dual-phase ADI – MG

Figure 7. RCF failure evolution in ADI – AG

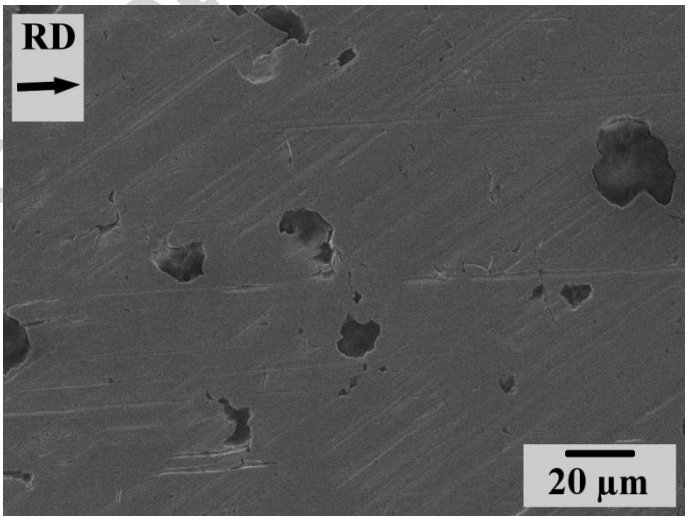

Figure 8. Surface micrograph inside the RT of ADI – AG indicating asperity contact

Figure 9 illustrates the Weibull plot of failure probability versus number of loading cycles for conventional ADI and dual-phase ADI. The results of the Weibull analysis are summarized in Table 2, reflecting shape parameter (β), characteristic life or scale parameter (η) and coefficient of determination (R^2). The characteristic lives of the tested samples can be ranked as follows: dual-phase ADI – MG > ADI – AG > dual-phase ADI – AG > ADI – MG. It can be seen that there is no a clear trend about the influence of the matrix microstructure on their RCF endurance neither about the surface finishing method of the samples.

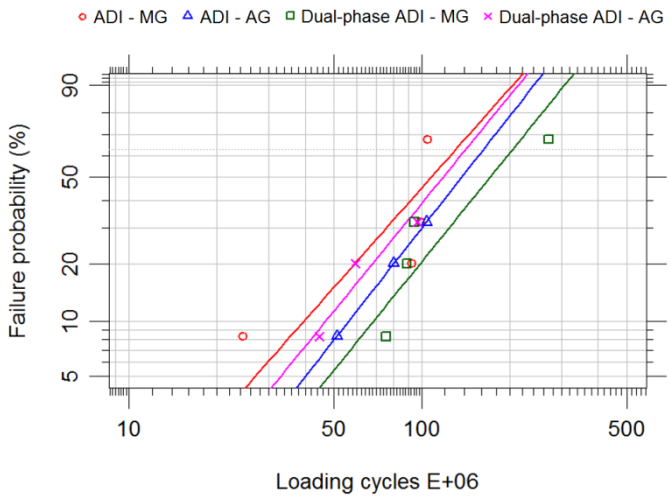

Figure 9. Weibull plot for ADI and dual-phase ADI

Table 2. Estimates of the Weibull parameters

Sample	β	η (cycles x10^6)	R^2
ADI – MG	1.88	130.8	0.672
ADI – AG	2.12	162.6	0.999
Dual-phase ADI – MG	2.05	204.4	0.809
Dual-phase ADI – AG	2.04	141.4	0.911

Table 3 compares the Weibull and Weibayes estimates of L10 for ADI and dual-phase ADI samples as a validity check of the Weibayes solution. Two-sided 90 % confidence intervals, determined by the Weibayes Method, are also reported. It can be seen that both solutions

provide similar values of L10 for each sample set, confirming the validity of the Weibayes solution. As with the characteristic life, the estimated L10 lives of the samples can be ranked as follows: dual-phase ADI – MG > ADI – AG > dual-phase ADI – AG > ADI – MG. The estimated confidence intervals confirm that there are no significant differences in the RCF endurance of ADI and dual-phase ADI although it has been reported that RCF crack propagation is driven by mode I stress intensity and that dual-phase ADI with a predominantly ausferritic microstructure displayed a higher mode I fracture toughness than conventional ADI [15, 30]. Consequently, it can be said that the presence of dispersed ferrite (soft points) in the matrix of dual-phase ADI does not significantly affect its RCF endurance. This behavior suggests that RCF life would be dominated by crack nucleation stage, as in a previous study [6], due to the fact that surface and subsurface graphite nodules act as defects where cracks easily nucleates. On the other hand, no differences in the RCF endurance attributable to the surface finishing method were identified either. This behavior can be ascribed to the fact that automatic grinding conditions do not promote a significant surface hardening. In addition, the depth of the plastically deformed layer (≈ 5 μm) is smaller than the depth of maximum shear stresses (30 μm), calculated according the Hertz contact theory.

Table 3. Weibull and Weibayes estimates of L10 and 90 % confidence intervals

Sample	Weibull Estimate (cycles x10^6)	Weibayes Estimate (cycles x10^6)	Weibayes confidence interval (cycles x10^6)
ADI – MG	39.52	40.29	28.33 – 71.34
ADI – AG	56.16	52.91	37.30 – 97.70
Dual-phase ADI – MG	68.32	62.09	44.96 – 104.85
Dual-phase ADI – AG	46.86	47.06	32.72 – 89.01

Taking into account the results of the present study and results of previous studies [15, 21], it can be said that dual-phase ADI with a predominantly ausferritic microstructure provides

improvements in ductility, friction coefficient and sliding wear resistance without reducing RCF life. However, further studies should be done in order to interpret the mechanisms of RCF crack nucleation and growth in ADI with dual-phase microstructures.

4. Conclusions

Dual-phase ADI structures with approximately 94 % of ausferrite and 6% of free aliotromorphic ferrite were obtained from fully ferritic microstructures. The surface properties and RCF behavior of dual-phase ADI were studied and compared to that of conventional ADI. The effect of the surface finishing (manual vs. automatic grinding) on the surface properties and RCF endurance was also analyzed. Based on the results obtained, the following conclusions can be drawn:

- The surface hardness of conventional ADI was higher than that of dual-phase ADI. The residual stresses were compressive in all the cases with similar average values for ADI and dual-phase ADI. With respect to manual grinding, the automatic process increased slightly the surface hardness and reduced by around a 50 % the residual stresses of both ADI and dual-phase ADI.
- Regarding RCF, failures in conventional ADI and dual-phase ADI were characterized by the typical concentrated damage in the form of spalls, which exhibit an irregular morphology influenced by the nodules present at and under the surface. No significant differences in the RCF endurance of ADI and dual-phase ADI were observed. No differences in the RCF endurance attributable to the surface finishing method were identified either.
- Since RCF endurance of dual-phase ADI with a predominantly ausferritic microstructure and small amount of free allotriomorphic ferrite in its microstructure is similar to that of

conventional ADI, it is worth noting that the replacement of ADI parts by this kind of dual-phase ADI is feasible, at least as far as rolling contact applications are concerned.

Acknowledgments

The financial support granted by the CONICET (Grant numbers PIP 11220110100558, PIP 11220150100756), the ANPCYT (Grant number PICT 2013-2630) and the National University of Mar del Plata (Grant number 15/G394) is gratefully acknowledged.

References

[1] T.E. Prucha, Cast Irons, ASM Handbook, Volume 15 - Casting, ASM International, Materials Park, Ohio, USA, 2008, pp. 783-907.

[2] P. David, J. Massone, R. Boeri, J. Sikora, Mechanical properties of thin wall ductile iron–influence of carbon equivalent and graphite distribution, ISIJ Int. 44 (2004) 1180-1187.

[3] R.B. Gundlach, J.F. Janowak, Austempered Ductile Irons Combine Strength with Toughness and Ductility, Met. Prog. 128 (1985) 19-26.

[4] J.R. Keough, ADI: ideal for high–strength, high–wear applications, Eng. Cast. Solut. 3 (2001) 42-44.

[5] R.A. Martinez, R.E. Boeri, J.A. Sikora, Impact and fracture properties of ADI, compared with SAE 4140 steel, Trans. Am. Foundry Soc. 106 (1998) 27-30.

[6] R.C. Dommarco, P.C. Bastias, H.A. Dall'O, G.T. Hahn, C.A. Rubin, Rolling Contact Fatigue (RCF) resistance of Austempered Ductile Iron (ADI), Wear 221 (1998) 69-74.

[7] L. Magalhães, J. Seabra, C. Sá, Experimental observations of contact fatigue crack mechanisms for austempered ductile iron (ADI) discs, Wear 246 (2000) 134-148.

[8] R.C. Dommarco, J.D. Salvande, Contact fatigue resistance of austempered and partially chilled ductile irons, Wear 254 (2003) 230-236.

[9] R.C. Dommarco, A.J. Jaureguiberry, J.A. Sikora, Rolling contact fatigue resistance of ductile iron with different nodule counts and matrix microstructures, Wear 261 (2006) 172-179.

[10] B. Wang, M. He, G.C. Barber, J.D. Schall, C. Tao, X. Sun, Rolling contact fatigue resistance of austempered ductile iron processed at various austempering holding times, Wear 398-399 (2018) 41-46.

[11] C. Brunetti, M.V. Leite, G. Pintaude, Effect of specimen preparation on contact fatigue wear resistance of austempered ductile cast iron, Wear 263 (2007) 663-668.

[12] V.K. Sharma, Roller contact fatigue study of austempered ductile iron, Journal of Heat Treating 3 (1984) 326-334.

[13] X. De-Xiang, L. Guang-Xi, Contact fatigue behaviour of an austenitic-bainitic ductile iron, Wear 169 (1993) 153-159.

[14] J. Aranzabal, G. Serramoglia, C.A. Goria, D. Rousière, Development of a new mixed (ferritic-ausferritic) ductile iron for automotive suspension parts, Int. J. Cast Met. Res. 16 (2003) 185-190.

[15] A.D. Basso, R.A. Martínez, J.A. Sikora, Influence of austenitising and austempering temperatures on microstructure and properties of dual phase ADI, Materials Science and Technology 23 (2007) 1321-1326.

[16] Y. Sahin, M. Erdogan, V. Kilicli, Wear behavior of austempered ductile irons with dual matrix structures, Mater. Sci. Eng., A 444 (2007) 31-38.

[17] A. Basso, R. Martínez, J. Sikora, Influence of section size on dual phase ADI microstructure and properties: comparison with fully ferritic and fully ausferritic matrices, Materials Science and Technology 25 (2009) 1271-1278.

[18] A. Basso, M. Caldera, iacute, M. Chapetti, J. Sikora, Mechanical Characterization of Dual Phase Austempered Ductile Iron, ISIJ Int. 50 (2010) 302-306.

[19] A. Basso, R. MartÍNez, A.P. Cisilino, J. Sikora, Experimental and numerical assessment of fracture toughness of dual-phase austempered ductile iron, Fatigue & Fracture of Engineering Materials & Structures 33 (2010) 1-11.

[20] I. Ovali, V. Kilicli, M. Erdogan, Effect of Microstructure on Fatigue Strength of Intercritically Austenitized and Austempered Ductile Irons with Dual Matrix Structures, ISIJ Int. 53 (2013) 375-381.

[21] H. Zhang, Y. Wu, Q. Li, X. Hong, Mechanical properties and rolling-sliding wear performance of dual phase austempered ductile iron as potential metro wheel material, Wear 406-407 (2018) 156-165.

[22] B. Zafošnik, Z. Ren, J. Flašker, G. Mishuris, Modelling of Surface Crack Growth under Lubricated Rolling–Sliding Contact Loading, International Journal of Fracture 134 (2005) 127-149.

[23] G.R. Miller, L.M. Keer, H.S. Cheng, On the mechanics of fatigue crack growth due to contact loading, Proceedings of the Royal Society of London. A. Mathematical and Physical Sciences 397 (1985) 197.

[24] L.M. Keer, M.D. Bryant, A Pitting Model for Rolling Contact Fatigue, J. Lubr. Technol. 105 (1983) 198-205.

[25] M. Kaneta, Y. Murakami, Effects of oil hydraulic pressure on surface crack growth in rolling/sliding contact, Tribol. Int. 20 (1987) 210-217.

[26] D.I. Fletcher, P. Hyde, A. Kapoor, Modelling and full-scale trials to investigate fluid pressurisation of rolling contact fatigue cracks, Wear 265 (2008) 1317-1324.

[27] A.F. Bower, The Influence of Crack Face Friction and Trapped Fluid on Surface Initiated Rolling Contact Fatigue Cracks, J. Tribol. 110 (1988) 704-711.

[28] X. Su, Surface initiated rolling/sliding contact fatigue in pearlitic and low/medium carbon bainitic steels, *PhD. Thesis*, Institute of Aeronautical Materials, Beijing China, 1996.

[29] P.E. Bold, M.W. Brown, R.J. Allen, A review of fatigue crack growth in steels under mixed mode I and II loading, Fatigue & Fracture of Engineering Materials & Structures 15 (1992) 965-977.

[30] R. Lancombe, A study of rolling contact fatigue cracks in lubricated contacts, *PhD. Thesis*, Imperial College London, 2012.

[31] M.C. Shaw, Principles of Abrasive Processing, Clarendon Press - Oxford, New York, USA, 1996.

[32] D.A. Colombo, M.D. Echeverría, O.J. Moncada, J.M. Massone, Characterisation of PVD–TiN coated austempered ductile iron: effects of nodule count and austempering temperature, ISIJ Int. 51 (2011) 448-455.

[33] ASTM A247-17, Standard Test Method for Evaluating the Microstructure of Graphite in Iron Castings, ASTM International, 2017.

[34] T.H. Kim, A.V. Olver, Stress history in rolling–sliding contact of rough surfaces, Tribol. Int. 31 (1998) 727-736.

[35] C.J. Smithells, E.A. Brandes, Metals Reference Book, 5th Edition ed., Butterworth, London, UK, 1976.

[36] D.A. Colombo, M.D. Echeverría, R.C. Dommarco, J.M. Massone, Influence of TiN coating thickness on the rolling contact fatigue resistance of austempered ductile iron, Wear 350–351 (2016) 82-88.

[37] K.L. Johnson, Contact Mechanics, Cambridge University Press, Cambridge, UK, 1987.

[38] G.T. Hahn, V. Bhargava, Q. Chen, The cyclic stress-strain properties, hysteresis loop shape, and kinematic hardening of two high-strength bearing steels, MTA 21 (1990) 653-665.

[39] D.A. Colombo, M.D. Echeverría, S. Laino, R.C. Dommarco, J.M. Massone, Rolling contact fatigue resistance of PVD CrN and TiN coated austempered ductile iron, Wear 308 (2013) 35-45.

[40] B.J. Hamrock, D. Dowson, Isothermal Elastohydrodynamic Lubrication of Point Contacts: Part III - Fully Flooded Results, J. Lubr. Technol. 99 (1977) 264-275.

[41] R.B. Abernethy, The New Weibull Handbook, 4th Edition ed., R.B. Abernethy, Florida, USA, 2000.

[42] J.I. McCool, Using the Weibull Distribution: Reliability, Modeling and Inference, Wiley, New Yersey, USA, 2012.

[43] A.D. Sosa, M.D. Echeverría, O.J. Moncada, N. Míngolo, J.A. Sikora, Influence of nodule count on residual stresses and distortion in thin wall ductile iron plates of different matrices, J. Mater. Process. Technol. 209 (2009) 5545-5551.

Highlights

- RCF behavior of dual-phase ADI was compared to that of conventional ADI.
- The effect of surface finishing (manual polishing vs. grinding) on RCF endurance was analyzed.
- RCF, failures were characterized by the typical concentrated damage in the form of spalls.
- No significant differences in the RCF endurance of ADI and dual-phase ADI were observed.
- No differences in the RCF endurance attributable to the surface finishing method were identified.